Onset of chaos in the rf-biased Josephson junction

R. L. Kautz
National Bureau of Standards, Boulder, Colorado 80303

J. C. Macfarlane
Division of Applied Physics, Commonwealth Scientific and Industrial Research Organization, Sydney, Australia 2070

(Received 26 July 1985)

The onset of chaos in the rf-biased Josephson junction is studied through numerical simulations. It is shown that the chaotic region predicted by the method of Melnikov spans only a narrow region of rf amplitudes and consists of weakly chaotic solutions which maintain phase lock with the rf bias. The experimentally observed threshold of chaos is shown to coincide with the onset of unlocked chaotic behavior at higher rf amplitudes.

I. INTRODUCTION

The existence of chaos in the rf-biased Josephson junction has been verified through theory,[1–5] simulation,[2,3,6–43] and experiment.[3,32,40,41,44,45] The extensive literature on chaos in this system is due in part to the fact that, when treated within the Stewart-McCumber model,[46,47] the equation of motion is one of the simplest to exhibit chaos and also describe a significant physical system. This situation allows chaos to be studied through a full interplay between theory, simulation, and experiment. The rf-biased junction is also of practical importance in that it defines a standard of voltage, an application for which chaotic behavior must be avoided.[38] In addition, what has been described as Josephson noise in SIS mixers[48] is very probably chaos in an rf-biased junction.

This paper is concerned with the onset of chaos in the Josephson junction at low levels of rf bias. The minimum rf amplitude required to produce chaos has been previously investigated theoretically,[1–5] in simulations,[2,3,7,10,13,16,18,25,29] and in experiments.[3,44] While there is reasonably good agreement between simulations and experiments for the rf-amplitude threshold of chaos,[3,44] theoretical predictions based on the method of Melnikov yield a significantly lower threshold.[2,3] This discrepancy has prompted the present study, in which numerical simulations are used to locate a narrow chaotic region, previously overlooked, for which the threshold of chaos is accurately predicted by the method of Melnikov. The onset of chaos is found by exploring the parameter range of periodic solutions and searching for bifurcations which lead either to the period-doubling scenario or the tangency scenario for chaos.[49] Bifurcation diagrams constructed for periodic solutions are used to show the relationship between the chaotic regions predicted by the method of Melnikov and those commonly observed in experiments and simulations.

The nature of the chaotic state is explored for a range of rf-bias levels near the onset of chaos. When the chaotic state is entered through a period-doubling sequence, it is found that the resulting state is one in which the junction phase maintains synchrony with the rf bias. As others have noted previously,[9,16,17,20,21,31,38] such phase-locked chaotic states typically span only a narrow parameter range. In agreement with Sakai and Yamaguchi,[31] we find that the phase-locked chaotic region is usually terminated by a crisis[50] which leads either to a region of periodic motion or a region of unlocked chaotic motion. The tangency scenario, on the other hand, often leads directly to unlocked chaotic motion.

The remainder of this paper may be outlined as follows. Section II reviews the results obtained by application of the method of Melnikov to the rf-biased junction. Sections III through V explore the parameter range of periodic solutions and the onset of chaos as a function of the bias frequency ω_1. The case in which ω_1 is much larger than the junction's plasma frequency ω_p is discussed in Sec. III. In this limit, stable periodic solutions are found to span a parameter range defined by the Bessel-function approximation and no chaotic behavior is observed. Section IV considers the situation in which ω_1 is greater than but comparable to ω_p. In this case, chaos is found to develop through a period-doubling cascade. Section V discusses values of ω_1 less than ω_p, in which case the onset of chaos may be associated either with tangency or with period doubling. Section VI explores the nature of the chaotic state near the onset of chaos.

II. METHOD OF MELNIKOV

Considered within the Stewart-McCumber model,[46,47] the system to be studied consists of an ideal Josephson element of critical current I_c shunted by a capacitance C and resistance R and driven by a current source which includes a dc component of amplitude I_0 and an rf component of amplitude I_1 and frequency ω_1. In terms of dimensionless parameters, the equation of motion for the junction phase ϕ is

$$\beta\ddot{\phi}+\dot{\phi}+\sin\phi=i_0+i_1\sin(\Omega_1\tau)\ , \tag{1}$$

where $\beta=2eI_cR^2C/\hbar$ is a dimensionless hysteresis parameter, $i_0=I_0/I_c$ is the normalized dc bias, $i_1=I_1/I_c$ is the normalized rf amplitude, $\Omega_1=\omega_1(\hbar/2eI_cR)$ is the normalized rf frequency, $\tau=t(2eI_cR/\hbar)$ is the normalized time, and dots indicate derivatives with respect to τ. In this notation $\dot{\phi}$ is the voltage across the junction normalized to I_cR. In addition to describing a Josephson junction, the above equation describes the motion of a damped, driven pendulum where ϕ is the angle of the pendulum from vertical.

The existence of chaos in the system defined by Eq. (1) is predicted theoretically by the method of Melnikov[49] for a special situation, namely the situation in which the system is close to being conservative and the motion is near a separatrix of the underlying conservative system. In the method of Melnikov, the nonconservative terms of the equation of motion, the damping and drive terms in the present case, are treated as perturbations. Although the predictions of the method of Melnikov are thus both limited and approximate, they are of interest because of the general scarcity of such analytical results in the theory of chaos.

The equation of motion for the conservative system underlying Eq. (1),

$$\beta\ddot{\phi}+\sin\phi=0 , \tag{2}$$

is equivalent to that of an undamped, undriven pendulum. Integrating Eq. (2) yields

$$E=\tfrac{1}{2}\beta\dot{\phi}^2+(1-\cos\phi) , \tag{3}$$

where the constant of integration E is the energy of the system in units of the Josephson coupling energy $\hbar I_c/2e$. Equation (3) defines the trajectories of the conservative system in state space, that is, in the $(\phi,\dot{\phi})$ plane. State-space trajectories are plotted in Fig. 1 for $\beta=100$ and several values of energy. Trajectories for $E<2$ correspond to a pendulum swinging back and forth, the energy being insufficient for the pendulum to reach the upward vertical position. For $E>2$ the motion corresponds to a pendulum rotating around and around, either in the forward or reverse direction depending on the initial conditions. The trajectory for $E=2$ is the separatrix. Motion on the separatrix corresponds to the case in which a pendulum begins in the upward vertical position with an infinitesimal velocity, gains speed as it falls toward the downward vertical, and comes to a stop as it approaches the upward vertical again. Because the velocity approaches zero at the beginning and end of the separatrix trajectory, the time required to traverse it from $-\pi$ to π is infinite. The method of Melnikov predicts the onset of chaos for situations in which the trajectories of the perturbed system approximate this motion.

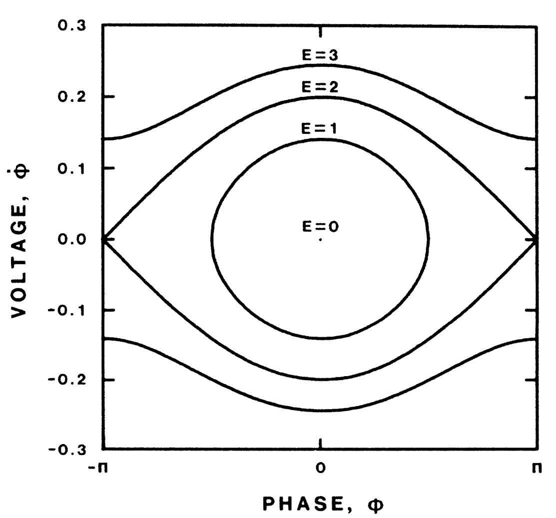

FIG. 1. State-space trajectories of the conservative system for $\beta=100$ and several values of energy.

When applied to Eq. (1), the method of Melnikov predicts that chaos will occur for rf amplitudes which exceed a critical value i_{1c} given by[2–4]

$$i_{1c}=\left|\frac{4}{\pi\sqrt{\beta}}\pm i_0\right|\cosh(\pi\tfrac{1}{2}\Omega_1\sqrt{\beta}) . \tag{4}$$

Simulations presented in the following sections confirm this result for the case $i_0=0$ and $\beta=100$ for a range of Ω_1.

The method of Melnikov is expected to be accurate only over parameter regions for which Eq. (1) represents a nearly conservative system. An estimate of this parameter region can be obtained if we require that the amounts of energy dissipated in the resistance and supplied by the current source over one excursion of the separatrix orbit are small compared to the total energy of the system. On the separatrix one notes that

$$\dot{\phi}=\frac{2}{\sqrt{\beta}}\cos(\phi/2) , \tag{5}$$

from which it follows that the energy dissipated in the resistance is

$$E_R=\int_{-\infty}^{\infty}\dot{\phi}^2\,d\tau=\int_{-\pi}^{\pi}\dot{\phi}\,d\phi=8/\sqrt{\beta} , \tag{6}$$

and the energy supplied by the dc source is

$$E_{\rm dc}=i_0\int_{-\infty}^{\infty}\dot{\phi}\,d\tau=i_0\int_{-\pi}^{\pi}d\phi=2\pi i_0 . \tag{7}$$

Requiring that E_R and $E_{\rm dc}$ be small compared to the total energy, $E=2$, yields

$$\beta\gg 16 , \tag{8}$$

$$i_0\ll 1/\pi . \tag{9}$$

Although it is not possible to obtain a simple expression for the energy supplied by the rf source, it is reasonable to assume that a condition similar to Eq. (9) must be imposed on i_1. Thus, we presume that the requirement

$$i_1\ll 1/\pi \tag{10}$$

and Eqs. (8) and (9) represent sufficient conditions for the validity of Eq. (4). These conditions are similar to but slightly more restrictive than those suggested by Gubankov *et al.*[3]

Further insight into the range of validity of Eq. (4) is obtained if one notes that the factor multiplying the cosh function is assured to be small by Eqs. (8) and (9) but the cosh function itself increases exponentially for large arguments. It follows that i_{1c} will generally satisfy Eq. (10) if and only if $\Omega_1\sqrt{\beta}$ is less than or on the order of unity. Because the junction's plasma frequency is $\Omega_p=1/\sqrt{\beta}$ in the dimensionless notation used here, Eq. (10) is roughly equivalent to the condition

$$\Omega_1 \lesssim \Omega_p \ . \tag{11}$$

Taken together, the conditions specified by Eqs. (8), (9), and (11) determine the range of parameters for which we might expect to find the onset of chaos predicted by the method of Melnikov. However, we begin our search by considering the limit $\Omega_1 \gg \Omega_p$ in order to make contact with a parameter region in which the range of periodic solutions approaches a simple form.

III. BESSEL-FUNCTION LIMIT

The presence of a periodic driving force suggests that the typical steady-state solutions of Eq. (1) will be periodic with a period equal to that of the rf-bias $2\pi/\Omega_1$ or possibly some multiple of this period. That is, we expect to find solutions which obey the relation

$$\phi(\tau + m\,2\pi/\Omega_1) = \phi(\tau) + 2\pi l \ , \tag{12}$$

for all τ with m and l integers. For such a solution, the phase advances by exactly l revolutions during m rf cycles and the average voltage $\langle \dot{\phi} \rangle$ is $(l/m)\Omega_1$. The smallest value of m for which Eq. (12) holds is the period of the solution measured in rf cycles.

For the rf-biased junction it is often found that the average voltage remains constant at a particular value of $(l/m)\Omega_1$ over some range of dc bias. On such rf-induced constant-voltage steps, the junction is said to be phase locked because the phase rotates in synchrony with the rf bias. It is useful to distinguish two types of rf-induced steps, namely principal steps, for which l/m is an integer n, and subharmonic steps, for which l/m is not an integer. It can be shown[6,51] that in the limit $\Omega_1 \gg 1$ or the limit $\Omega_1 \gg \Omega_p$, the principal step of order n spans the range of dc bias given by

$$n\Omega_1 - |J_n(\tilde{i}_1)| < i_0 < n\Omega_1 + |J_n(\tilde{i}_1)| \ , \tag{13}$$

where J_n is the Bessel function of order n and $\tilde{i}_1$ is an alternative measure of the rf amplitude defined by

$$\tilde{i}_1 = i_1 \Omega_1^{-1} (1 + \Omega_1^2 \beta^2)^{-1/2} \ . \tag{14}$$

Later in this section, we compare the computed range of periodic solutions for $\Omega_1 = 2\Omega_p$ with the limiting Bessel-function form given by Eq. (13).

The problem of finding periodic solutions to Eq. (1) is equivalent to the problem of finding initial conditions $\phi(0)$ and $\dot{\phi}(0)$ such that the computed trajectory yields

$$\phi(m\,2\pi/\Omega_1) = \phi(0) \ (\mathrm{mod}\,2\pi) \ , \tag{15}$$

and

$$\dot{\phi}(m\,2\pi/\Omega_1) = \dot{\phi}(0) \ , \tag{16}$$

where m is the expected period. An iterative approach to solving Eqs. (15) and (16) that has been discussed elsewhere[51] was employed in the present study. Because this method does not use the natural relaxation of the system to find steady-state solutions, it yields periodic solutions which are unstable as well as those which are stable. A knowledge of unstable solutions often proves to be useful in that an exploration of their parameter range can lead to the discovery of stable solutions which would otherwise be difficult to locate.

To distinguish stable periodic solutions from unstable ones, we test the local stability of each solution by computing its Liapunov exponents. If the state vector $(\phi,\dot{\phi})$ of a solution is represented by (X_1, X_2), then its Liapunov exponents λ_i are defined by[49]

$$\lambda_i = \lim_{\tau \to \infty} \left[\frac{1}{\tau - \tau_0} \ln |\, i\text{th eigenvalue of } \underline{J}(\tau,\tau_0) \,| \right] , \tag{17}$$

where $\underline{J}$ is the Jacobian matrix,

$$J_{ij}(\tau,\tau_0) = \frac{\partial X_i(\tau)}{\partial X_j(\tau_0)} \ . \tag{18}$$

Stability is determined by the maximum Liapunov exponent, which we denote by λ. For periodic solutions a negative λ implies stability and a positive λ implies instability. The numerical methods used to evaluate Liapunov exponents for this system have been discussed elsewhere.[38]

In the search for periodic solutions of Eq. (1) that approximate the separatrix trajectory of Eq. (2), it is possible to imagine two ways of obtaining a match. One possibility is a solution in which ϕ oscillates about zero with an oscillation amplitude approaching π and an oscillation period equal to the rf cycle. This solution corresponds to a point on the $n=0$ principal step. The second possibility

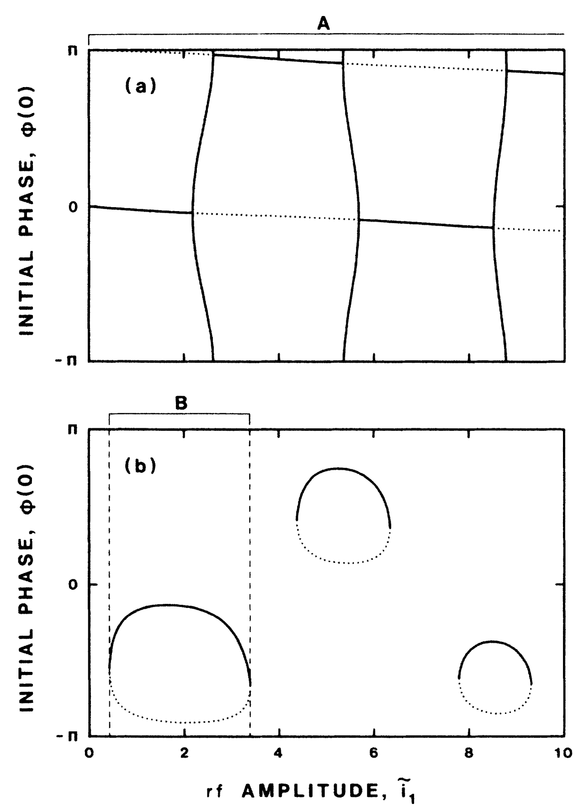

FIG. 2. Initial phase of period-1 solutions as a function of rf amplitude on the $n=0$ step (a) and $n=1$ step (b) for $\beta=100$, $\Omega_1=0.2$, and $i_0=0$. Stable and unstable solutions are indicated by solid and dotted lines, respectively.

is a solution in which ϕ advances by one revolution during each rf cycle and the angular velocity approaches close to zero as ϕ passes through π. This solution corresponds to a point on the $n=1$ principal step. These associations suggest that the chaotic region predicted by Eq. (4) will evolve out of $n=0$ or $n=1$ periodic solutions. In the following, attention is restricted to these cases.

The various periodic solutions for a given set of parameters β, Ω_1, i_0, and i_1 can be identified uniquely by specifying the state vector of a given point in the rf cycle, say $(\phi(0), \dot{\phi}(0))$. Although it leads to an occasional ambiguity, we will, for simplicity, identify periodic solutions solely by their initial phases $\phi(0)$. The initial phases of period-1 solutions are shown in Fig. 2 as a function of rf amplitude for the case $\beta=100$, $\Omega_1=0.2$, and $i_0=0$. The $n=0$ and $n=1$ solutions are shown in Figs. 2(a) and 2(b), respectively, with stable and unstable solutions indicated by solid and dotted lines, respectively. Figure 2 is called a bifurcation diagram and can be regarded as a catalog of periodic solutions.

Consider first the locus of $n=0$ solutions plotted in Fig. 2(a). In the absence of an rf bias there are two solutions, a stable one at $\phi(0)=0$ and an unstable one at $\phi(0)=\pi$. These solutions correspond to a pendulum at rest in the downward vertical position and a pendulum balanced in the upward vertical position. For small rf-bias levels the stable solution is one in which the pendulum simply oscillates symmetrically about $\phi=0$. Above $\tilde{i}_1=2.19$, this symmetric solution loses its stability and between $\tilde{i}_1=2.19$ and 2.63 there are two stable solutions, each of which violates the symmetry of the $i_0=0$ system. One of the two solutions corresponds to a pendulum swinging further in the positive ϕ direction than the negative ϕ direction. For the other solution this asymmetry is exactly reversed. The pair of solutions having broken symmetry develops through a pitchfork bifurcation at $\tilde{i}_1=2.19$ and vanishes again through a pitchfork bifurcation at $\tilde{i}_1=2.63$. Between $\tilde{i}_1=2.63$ and 5.36 the stable solution is again symmetric but the point of symmetry is $\phi=\pi$ rather than $\phi=0$. After a second interval of symmetry breaking between $\tilde{i}_1=5.36$ and 5.69, the stable solution returns to being symmetric about $\phi=0$. With further increases in $\tilde{i}_1$ the pattern of symmetric and asymmetric solutions begins to repeat itself. However, each time the solution symmetric about $\phi=0$ (or $\phi=\pi$) returns at a higher level of rf bias, the amplitude of the oscillation increases by about 2π. The $n=0$ solutions which most closely approximate the separatrix orbit are the solutions symmetric about $\phi=0$ near the first interval of broken symmetry where the oscillation amplitude approaches π.

Symmetry breaking in the $i_0=0$ system has previously been discussed by D'Humieres *et al.*[16] and MacDonald and Plishke.[18] It is easily verified that if $\phi_1(\tau)$ is a solution of Eq. (1), then the function

$$\phi_2(\tau)=-\phi_1(\tau+\pi/\Omega_1) \tag{19}$$

is also a solution in the case $i_0=0$. For the symmetric solutions discussed above, ϕ_1 and ϕ_2 are identical mod2π, but in the case of broken symmetry, ϕ_1 and ϕ_2 can be identified as the pair of asymmetric solutions.

It is useful to compare the range of $n=0$ solutions shown in Fig. 2(a) for $\Omega_1=2\Omega_p$ with the Bessel-function form given by Eq. (13). In the limit $\Omega_1 \gg \Omega_p$, Eq. (13) predicts the existence of an $n=0$ solution at $i_0=0$ provided $|J_0(\tilde{i}_1)|>0$. Thus, $n=0$ solutions are expected for all $\tilde{i}_1$ except the zeros of J_0. These exceptional points correspond to the points at which the limiting form of the solution switches between oscillations symmetric about $\phi=0$ and oscillations symmetric about $\phi=\pi$. Comparing this situation with the case of finite Ω_1 suggests that the zeros of J_0 will fall near the intervals of i_1 over which symmetry breaking is observed. Indeed, the first three zeros, $\tilde{i}_1=2.40$, 5.52, and 8.65, fall within the intervals of broken symmetry shown in Fig. 2(a). One concludes that this bifurcation diagram is very close to what would be obtained in the limit $\Omega_1 \gg \Omega_p$.

We now consider the $n=1$ solutions for $\Omega_1=2\Omega_p$ which span three distinct intervals of $\tilde{i}_1$ as shown in Fig. 2(b). Each interval is spanned by one stable and one unstable solution, the two solutions disappearing together at each end of the interval in a tangent or saddle-node bifurcation. Although tangent bifurcations sometimes lead to chaotic behavior, in the present instance the system simply switches from the $n=1$ state to the $n=0$ state as $\tilde{i}_1$ passes through the point of tangency and no chaos results.

An $n=1$ solution is necessarily asymmetric since ϕ increases by 2π during each rf cycle. The solution for which this asymmetry is reversed is an $n=-1$ solution and for each $n=1$ solution there is a corresponding $n=-1$ solution given by Eq. (19). Because both solutions span the same range of $\tilde{i}_1$, it is sufficient to consider only the $n=1$ solution.

As with the $n=0$ solutions for $\Omega_1=2\Omega_p$, the ranges of $\tilde{i}_1$ spanned by the $n=1$ solutions are given approximately by the Bessel-function limit. From Eq. (13) we expect stable $n=1$ solutions at $i_0=0$ provided $|J_1(\tilde{i}_1)|>\Omega_1$. For the case $\Omega_1=0.2$, Eq. (13) thus predicts $n=1$ solutions between $\tilde{i}_1=0.41$ and 3.35, between $\tilde{i}_1=4.39$ and 6.33, and between $\tilde{i}_1=7.79$ and 9.30, in close agreement with the results shown in Fig. 2. The nature of the solutions on each of these three intervals is distinctly different. Roughly speaking, on the first interval ϕ advances by 2π during each rf cycle without any backward rotation. On the second interval a net advance of 2π is obtained by rotating forward 4π and then backward 2π during each rf cycle. On the third interval ϕ rotates forward 6π then backward 4π. Of these three types of motion, it is the one on the first interval which is expected to approximate the separatrix orbit.

Because chaotic behavior is not observed at $\Omega_1=2\Omega_p$ and the solutions at this frequency already approximate the limit $\Omega_1 \gg \Omega_p$, it is reasonable to conclude that chaos will not be observed for Ω_1 greater than $2\Omega_p$. In the following sections we explore the range of $n=0$ and $n=1$ solutions for Ω_1 less than $2\Omega_p$. Attention will be focused on two solution branches, to be designated A and B. Branch A is defined, for the present, to include the stable $n=0$ solution at $\tilde{i}_1=0$ and all stable $n=0$ solutions which can be reached from this solution by a continuous tracing through stable solutions on the bifurcation diagram. At $\Omega_1=2\Omega_p$, branch A apparently spans the range from $\tilde{i}_1=0$ to infinity. Branch B is similarly defined to include the stable $n=1$ solution of lowest $\tilde{i}_1$ and all the stable $n=1$ solutions connected to it through stable solutions by the bifurcation diagram. At $\Omega_1=2\Omega_p$, branch B extends from $\tilde{i}_1=0.43$ to 3.39. The ranges of branches A and B are indicated in Fig. 2 by brackets at the top of the frames.

At this point it is useful to introduce Fig. 3, which summarizes the results of this and the following sections. Figure 3 shows the frequency dependence of the rf-amplitude ranges of solution branches A and B plus that of a third branch, designated C, which is defined later. In addition, the onset of chaos predicted by the method of Melnikov is shown by a dashed line. The rf amplitude is plotted here as i_1 rather than $\tilde{i}_1$ to simplify comparison with the results of previous workers. Figure 3 will be discussed in detail as we examine a succession of bifurcation diagrams for frequencies less than $2\Omega_p$.

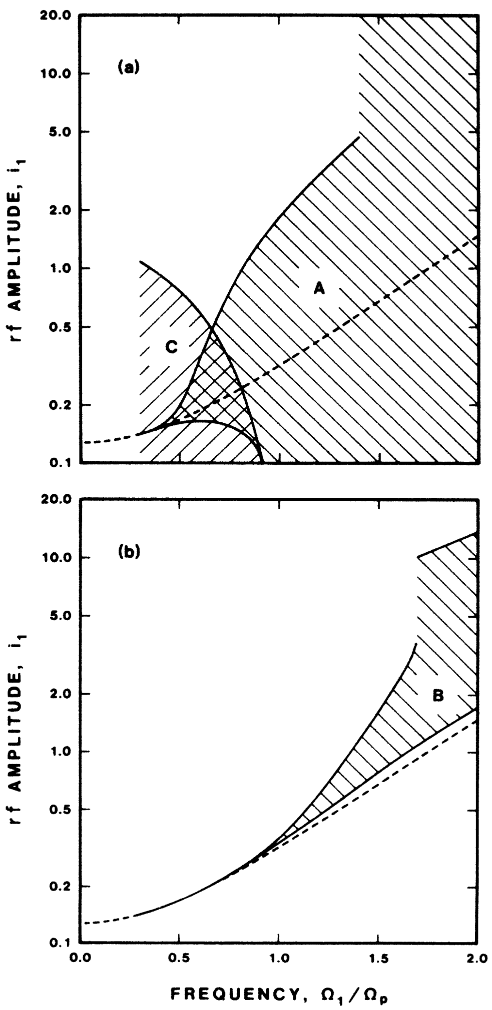

FIG. 3. Range of rf amplitude for solution branches A, B, and C as a function of frequency for $B=100$ and $i_0=0$. For clarity, the $n=0$ and $n=1$ solutions are shown separately in frames (a) and (b), respectively. The dashed line in each frame indicates the onset of chaos predicted by Eq. (4).

IV. PERIOD-DOUBLING CASCADE

Bifurcation diagrams for period-1 solutions on the $n=0$ and $n=1$ steps are shown in Figs. 4(a) and 4(b), respectively, for $\Omega_1=1.4\Omega_p$. These diagrams are like those shown in Fig. 2 for $\Omega_1=2\Omega_p$ with the exception of two regions where stable solutions are replaced by unstable solutions. In particular, the $n=0$, $m=1$ solution is unstable over the range from $\tilde{i}_1=2.30$ to 2.66 in the first region of broken symmetry and the $n=1$, $m=1$ solution is unstable over the range from $\tilde{i}_1=0.52$ to 2.63 in the first interval over which it is expected to be stable. These instabilities are associated with the onset of chaos through period doubling, a situation observed many times previously in this system.[7,9,13,15–18,20,22,25,27,31]

The regions of instability on the $n=0$ and $n=1$ steps are shown on expanded scales in Fig. 5. In order to illustrate the period-doubling bifurcation cascade, this figure includes period-2 and period-4 solutions in addition to the period-1 solutions shown in Fig. 4. As an example of period doubling, consider the $n=0$ solutions having positive initial phase in Fig. 5(a). At $\tilde{i}_1=2.298$, where the $m=1$ solution loses stability, there is a pitchfork bifurcation and two stable $m=2$ solutions appear. The $m=2$ solutions become unstable at $\tilde{i}_1=2.372$ and pitchfork bifurcations at this point lead to four stable $m=4$ solutions. The $m=4$ solutions become unstable in turn at $\tilde{i}_1=2.387$ and pitchfork bifurcations at this point lead to eight $m=8$ solutions (not shown). An exactly similar

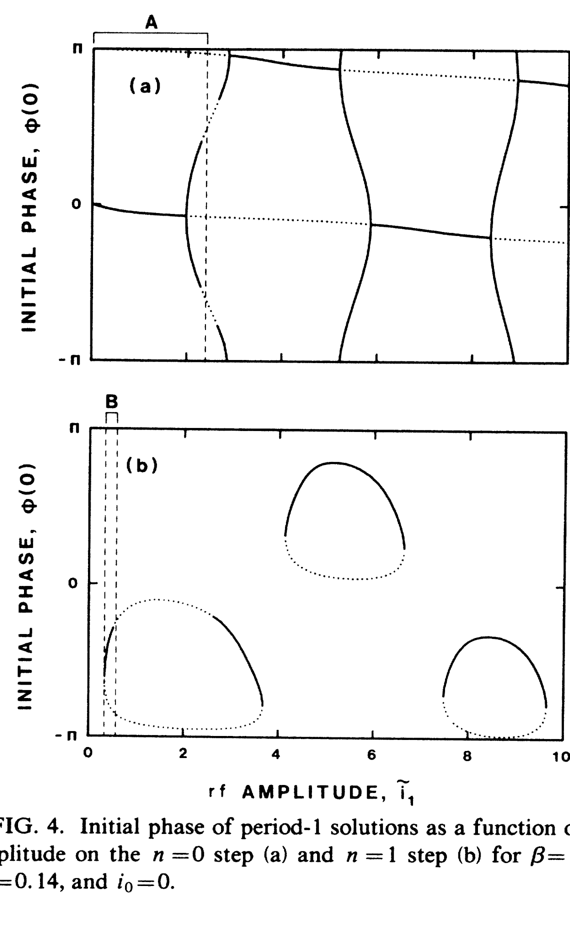

FIG. 4. Initial phase of period-1 solutions as a function of rf amplitude on the $n=0$ step (a) and $n=1$ step (b) for $\beta=100$, $\Omega_1=0.14$, and $i_0=0$.

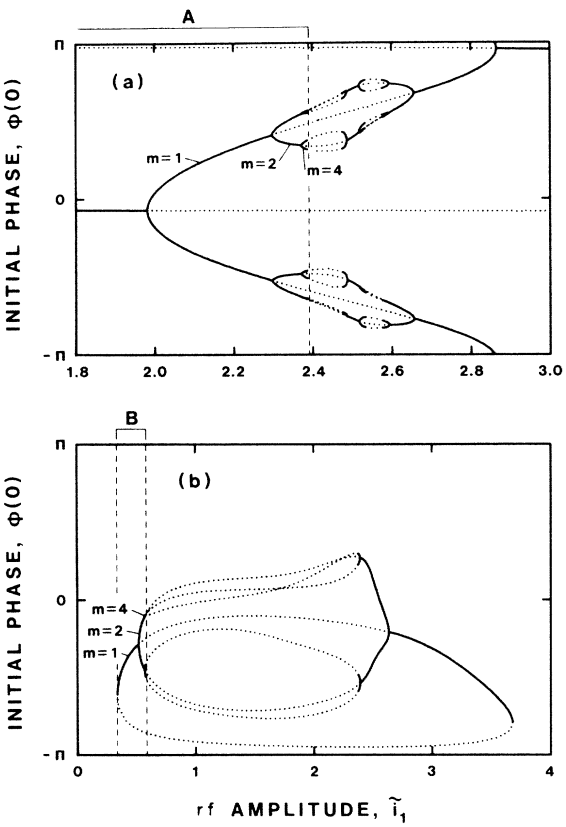

FIG. 5. Initial phase as a function of rf amplitude for solutions of period 1, 2, and 4 on the $n=0$ step (a) and $n=1$ step (b) for $\beta=100$, $\Omega_1=0.14$, and $i_0=0$.

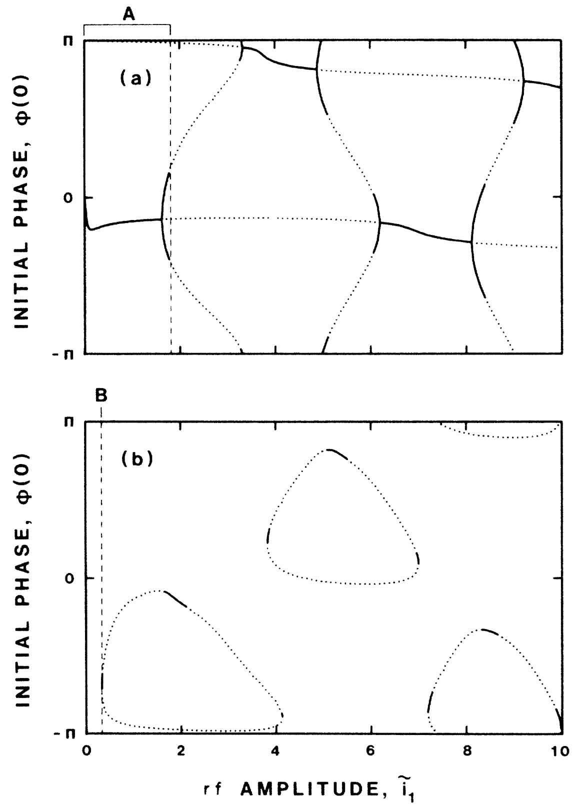

FIG. 6. Initial phase as a function of rf amplitude for period-1 solutions on the $n=0$ step (a) and $n=1$ step (b) for $\beta=100$, $\Omega_1=0.1$, and $i_0=0$.

period-doubling sequence occurs for the $n=0$ solutions with reversed asymmetry having negative initial phases.

In the period-doubling cascade, the interval $\Delta\tilde{i}_1(m)$ over which the solution of period m is stable decreases rapidly with increasing m. In fact, general arguments show that[49]

$$\lim_{k\to\infty} \frac{\Delta\tilde{i}_1(2^k)}{\Delta\tilde{i}_1(2^{k+1})} = 4.6692\ldots\,, \tag{20}$$

where 4.6692... is a universal constant. Equation (20) allows one to estimate the accumulation point of the cascade $\tilde{i}_{1c}$, at which the period of the solution approaches infinity and beyond which the motion of the system becomes chaotic. Based on the stability interval of the period-8 solution, $\tilde{i}_{1c}$ is estimated to be 2.391 for the $n=0$ cascade discussed above. This value of $\tilde{i}_1$ defines the upper limit of solution branch A at $\Omega_1=1.4\Omega_p$ and is a threshold for chaotic behavior, as will be verified in Sec. VI. Similarly, as shown in Fig. 5(b), solution branch B ends in a period-doubling cascade with a threshold for chaos at $\tilde{i}_{1c}=0.581$. As can be seen from Fig. 3, these values of $\tilde{i}_1$ for the onset of chaos are significantly above the threshold of 0.296 predicted by the method of Melnikov. However, as Eq. (11) indicates, the method of Melnikov is not expected to be especially accurate at $\Omega_1=1.4\Omega_p$.

The breakdown in stability of the $n=0$ and $n=1$ solutions which leads to chaotic behavior at $\Omega_1=1.4\Omega_p$ was not observed at $\Omega_1=2\Omega_p$. At what value of Ω_1 does chaotic behavior first occur? Chaos is found to first evolve out of the $n=0$ solution at a point between $\Omega_1=1.41\Omega_p$ and 1.40 Ω_p and out of the $n=1$ solution between $\Omega_1=1.70\Omega_p$ and $1.69\Omega_p$. These critical values of Ω_1 are evidenced in Fig. 3 by discontinuities in the range of solution branches A and B. The results shown in Fig. 3 confirm the empirical rule[9,38] that chaos does not occur in this system for $\Omega_1 \gg \Omega_p$.

The bifurcation diagrams for period-1 solutions on the $n=0$ and $n=1$ steps are shown for $\Omega_1=\Omega_p$ in Fig. 6. Although similar to the results for $\Omega_1=1.4\Omega_p$, these diagrams reveal several additional regions of instability. In Fig. 6(a), all three of the intervals of broken symmetry show instabilities and, in Fig. 6(b), all three of the $n=1$ solution intervals include unstable regions. Because Fig. 6 includes only $m=1$ solutions, the pitchfork bifurcations shown here are all associated with symmetry breaking. However, if one excludes from consideration all of the pitchfork and tangent bifurcations displayed in Fig. 6, then all other points at which the $m=1$ solution loses stability are points at which period-doubling cascades are initiated. Viewed with this fact in mind, Fig. 6(a) suggests that intervals of chaos will alternate with intervals of stable period-1 solutions as a function of increasing rf amplitude. This regular alternation between periodic and chaotic solutions, noted previously by Octavio,[25] derives from the system's tendency, still apparent in Fig. 6, to follow the Bessel-function pattern.

At $\Omega_1=\Omega_p$, solution branches A and B are qualitatively similar to what they are at $\Omega_1=1.4\Omega_p$, but the range of branch B is very small, as shown in Fig. 6(b). The accumulation points which terminate branches A and B at their upper limits are $\tilde{i}_{1c}=1.808$ and 0.352, respectively, at $\Omega_1=\Omega_p$. The latter value is reasonably close to the threshold of 0.318 predicted by the method of Melnikov. In the next section it is shown that, for values of Ω_1 less than Ω_p, the method of Melnikov becomes an accurate predictor of the accumulation points of both the $n=0$ and $n=1$ cascades.

V. HYSTERESIS AND TANGENCY

Bifurcation diagrams for the case $\Omega_1=0.7\Omega_p$ are shown in Fig. 7. An important new feature of the $n=0$ diagram is a region of hysteresis between $\tilde{i}_1=0$ and the end of the first period-doubling cascade at $\tilde{i}_1=1.177$. The stable $n=0$ solution branch beginning at $\tilde{i}_1=0$ ends at $\tilde{i}_1=0.851$ with a tangent bifurcation. If $\tilde{i}_1$ is increased beyond 0.851, the system jumps to a second solution branch which ranges from $\tilde{i}_1=0.324$, where it begins with a tangent bifurcation, to $\tilde{i}_1=1.177$, the end of the period-doubling cascade. The hysteresis loop is completed if $\tilde{i}_1$ is reduced below 0.324, forcing the system to switch from the second branch back to the first. For reasons of continuity, we retain the label A for the branch ending with the period-doubling cascade and introduce the label C for the branch that begins at $\tilde{i}_1=0$. The range of solution

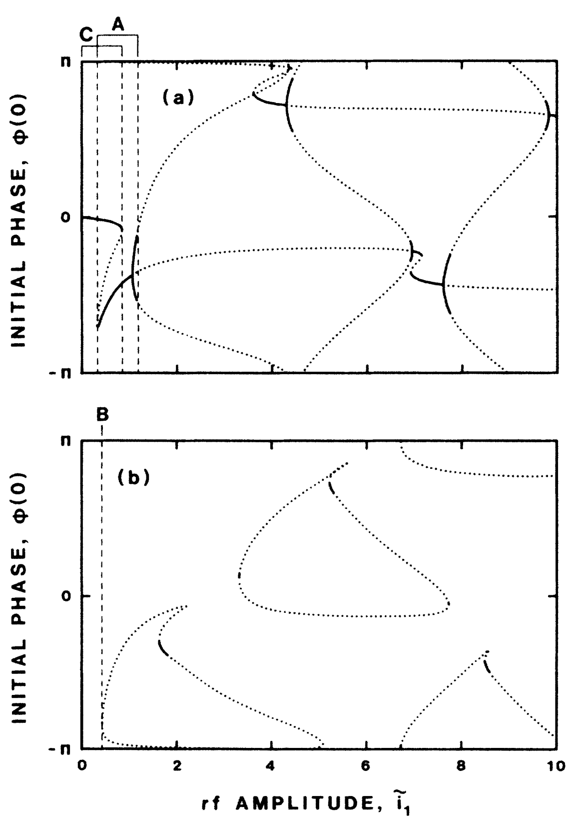

FIG. 7. Initial phase as a function of rf amplitude for period-1 solutions on the $n=0$ step (a) and $n=1$ step (b) for $\beta=100$, $\Omega_1=0.07$, and $i_0=0$.

branches A and C are indicated by brackets at the top of Fig. 7(a).

The hysteresis region described above has been considered previously by Huberman *et al.*[7] and D'Humieres *et al.*[16] The ranges of solution branches A and C are shown as a function of frequency in Fig. 3(a). The region of hysteresis is the roughly triangular area where branches A and C overlap. Branch C first appears at frequencies just below $\Omega_1=\Omega_p$. The initiation of branch C can be seen in the bifurcation diagram for $\Omega_1=\Omega_p$ [Fig. 6(a)] as the apparently infinite slope of branch A at $\tilde{i}_1=0$. At frequencies below Ω_p, branch C expands rapidly to cover a broad range of rf amplitudes while branch A narrows until it spans only a very small range of $\tilde{i}_1$ at 0.3 Ω_p, the lowest frequency simulated.

At frequencies below Ω_p, the character of the solutions on branch A is determined by a resonance between the drive frequency and the natural oscillation modes of the system.[16] To understand this resonance effect, it is useful to consider again the undamped, undriven system of Eq. (2). In the limit of small oscillation amplitudes ($E\to 0$), the oscillation period of the conservative system approaches $2\pi/\Omega_p$. The system's nonlinearity gives rise to longer periods of oscillation for larger oscillation amplitudes, with the period approaching infinity as the amplitude approaches π ($E\to 2$). Quantitatively, the orbital period τ_0 is given by

$$\tau_0=\frac{4}{\Omega_p}K(\phi_0/2)\,, \tag{21}$$

where K is the complete elliptic integral of the first kind with modular-phase argument[52] and $\phi_0=\cos^{-1}(1-E)$ is the oscillation amplitude. At any drive frequency less than Ω_p, there will be some oscillation amplitude for which the orbital period of the conservative system matches the drive period. Thus, if the damped, driven system is not heavily damped, we might expect to find resonant solutions for a range of rf amplitudes producing orbits with natural periods which approximate the rf drive period.

To confirm that the solutions on branch A are the proposed resonant solutions, we consider the computed solutions at $\Omega_1=0.7\Omega_p$. Figure 8 shows state-space trajectories for an rf amplitude at which stable period-1 solutions exist simultaneously on branches A, B, and C. The resonant nature of solution A is suggested by the fact that its orbit is much larger than that of solution C. More conclusive evidence is given by the near coincidence of the amplitude of solution A, namely $\phi_0=2.34$, with the amplitude predicted by Eq. (21) for a conservative orbit having the same period, namely $\phi_0=2.20$.

In addition to confirming the resonant nature of branch A, Fig. 8 allows us to compare the state-space trajectories of solutions A and B with the separatrix, which is indicated by a dotted line. Although both solutions lie near the separatrix, solution B is significantly closer than solution A. This difference correlates with the fact that the end point of the period-doubling cascade for branch B, $\tilde{i}_{1c}=0.431$, is much closer to the threshold of chaos predicted by the method of Melnikov, $\tilde{i}_{1c}=0.429$, than the end point of the cascade for branch A, $\tilde{i}_{1c}=1.177$.

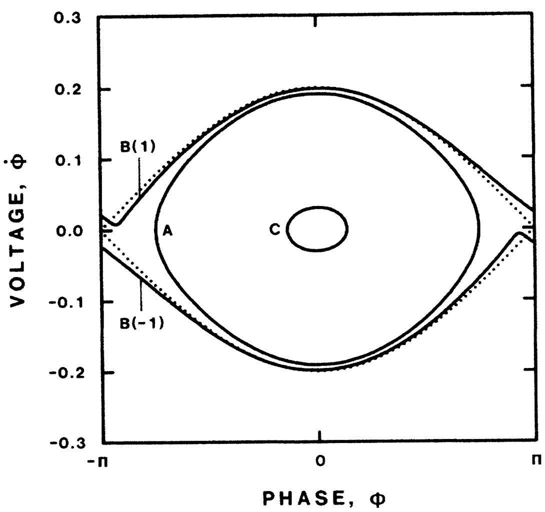

FIG. 8. State-space trajectories for period-1 solutions on branches A, B, and C for $\beta=100$, $\Omega_1=0.07$, $i_0=0$, and $\tilde{i}_1=0.4312$. Both the $n=1$ and $n=-1$ trajectories are shown for branch B. The separatrix of the conservative system is indicated by a dotted line.

The rapid convergence of branch B to the separatrix orbit with decreasing Ω_1, relative to branch A, can be understood in terms of the difference in the distance to be traversed in ϕ space for the two orbits. For an $n=1$ solution which approximates the separatrix, the system moves from $-\pi$ to π during one rf cycle while for an $n=0$ solution the system must move from $-\pi$ to π and back to $-\pi$ again in the same period of time. At $\Omega_1=0.7\Omega_p$ the rf cycle is sufficiently long for an $n=1$ solution to traverse the separatrix once but not sufficiently long for an $n=0$ solution to do so twice. This factor of 2 explains why the threshold predicted by the method of Melnikov is rapidly approached by the upper limit of branch B for frequencies below Ω_p while it is approached by the upper limit of branch A only below 0.5 Ω_p, as shown in Fig. 3.

Bifurcation diagrams for the case $\Omega_1=0.5\Omega_p$ are shown in Fig. 9. Here we find that the upper bounds of branches A and B are nearly coincident. The state-space trajectories shown in Fig. 10 reveal that solutions A and B both approach the separatrix orbit very closely. Thus, it is not surprising to find that the end points of the cascade for branches A and B, $\tilde{i}_{1c}=0.779$ and 0.661, are both close to the threshold for chaos predicted by Eq. (4), $\tilde{i}_{1c}=0.662$. At $\Omega_1=0.3\Omega_p$, the agreement is even better, with a predicted threshold of $\tilde{i}_{ic}=1.494$ and observed accumulation points at $\tilde{i}_{1c}=1.490$ and 1.491 for branches A and B.

Experimentally, solution branches A and B would be difficult to observe at $\Omega_1=0.5\Omega_p$. As Fig. 9(a) indicates, the system starts on solution branch C at $\tilde{i}_1=0$ and will remain on branch C as $\tilde{i}_1$ is increased up to 2.99, a point well beyond the ranges of branches A and B. Thus, the experimentally observed threshold of chaos will be at or beyond the tangent bifurcation which terminates branch C. As Fig. 3 shows, this situation holds for frequencies below $\Omega_1=0.66\Omega_p$, the crossover point between the upper limits of branches A and C. In some cases, including that shown in Fig. 9(a), another stable solution branch overlaps

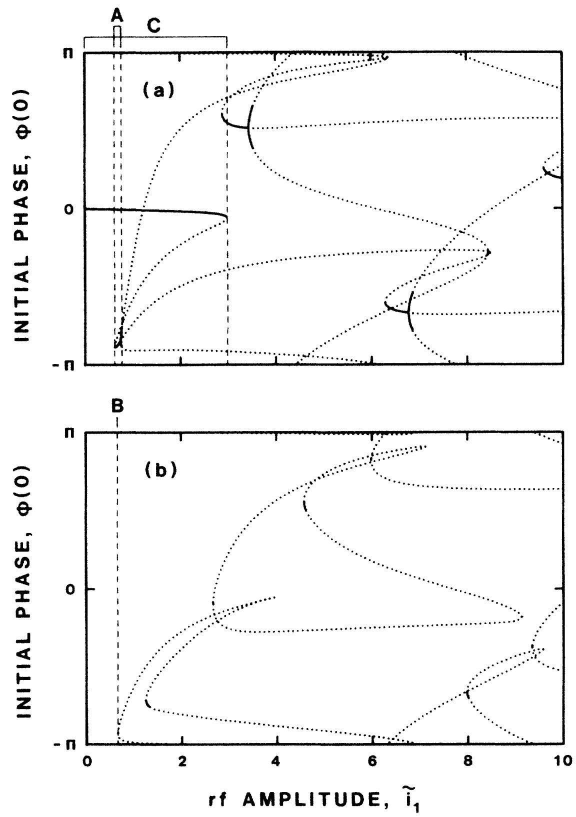

FIG. 9. Initial phase as a function of rf amplitude for period-1 solutions on the $n=0$ step (a) and $n=1$ step (b) for $\beta=100$, $\Omega_1=0.05$, and $i_0=0$.

the upper limit of branch C and the system merely switches to another type of periodic motion when $\tilde{i}_1$ passes through the point of tangency. In other cases, no such periodic solution exists and the system enters the chaotic state when the upper limit of branch C is exceeded. In fact, at frequencies below $\Omega_1=0.66\Omega_p$, the ob-

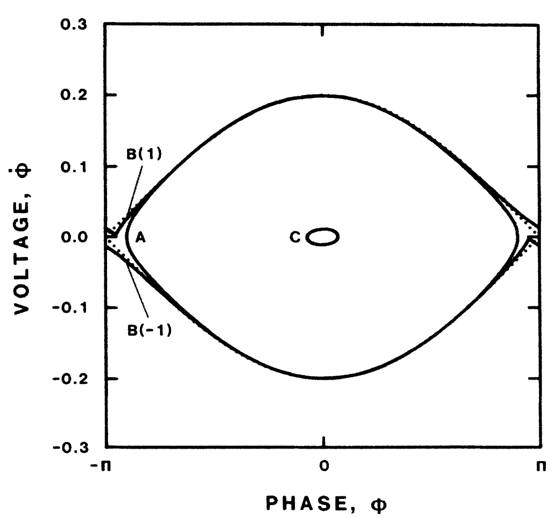

FIG. 10. State-space trajectories for period-1 solutions on branches A, B, and C for $\beta=100$, $\Omega_1=0.05$, $i_0=0$, and $\tilde{i}_1=0.661083$. The separatrix of the conservative system is indicated by a dotted line.

served threshold of chaos is often the tangent bifurcation at the end of solution branch C. An example in which the chaotic state is entered through the tangency scenario in this way will be discussed in the next section.

VI. CHAOS

In the previous discussion, the onset of chaos has been explored through bifurcation diagrams for periodic solutions. In this section we examine the chaotic state itself in the region near the threshold of chaos.

A bifurcation diagram which includes chaotic solutions is shown in Fig. 11(a) for a case in which chaos develops through a period-doubling cascade. Fig. 11(a) continues the bifurcation sequence shown in Fig. 5(a) to solutions with periods greater than 4. The procedure used to construct Fig. 11(a) consists of first allowing the system to relax to the steady-state solution at a given rf amplitude and then plotting the phase at the beginning of 512 successive rf cycles. In the region below $\tilde{i}_1=2.3873$, where the steady-state solution has a period of 4 rf cycles, this procedure yields all four possible values of initial phase. Between $\tilde{i}_1=2.3873$ and 2.3902 one finds eight different values of initial phase, indicating a period-8 solution. At higher values of $\tilde{i}_1$ the period-doubling process continues with solutions having periods of 16, 32, 64, ..., rf cycles.

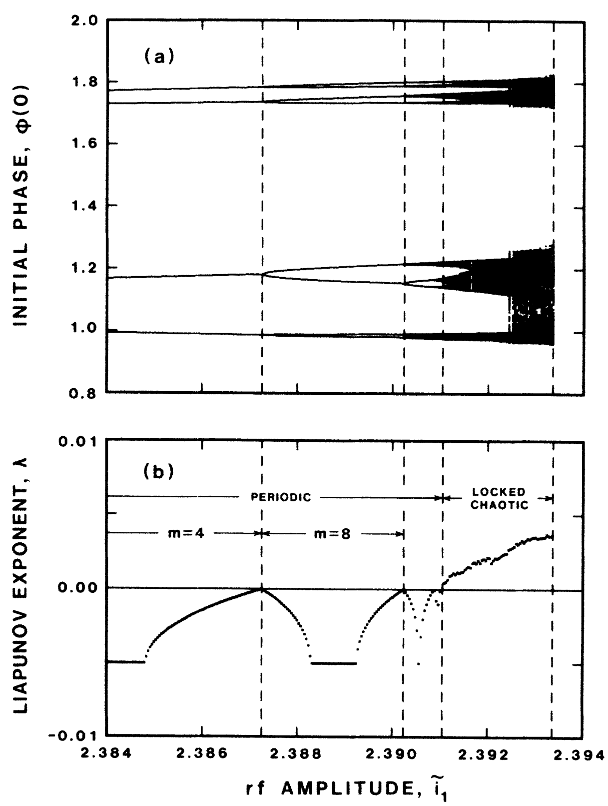

FIG. 11. Initial phase (a) and maximum Liapunov exponent (b) of the steady-state solution as a function of rf amplitude for $\beta=100$, $\Omega_1=0.14$, and $i_0=0$. For each rf amplitude, the phase at the beginning of 512 successive rf cycles is plotted in frame (a). The maximum Liapunov exponent is calculated over 8192 rf cycles.

Beyond the accumulation point of the cascade at $\tilde{i}_1=2.3910$, the period of the solution is presumably infinite and the 512 plotted points merely give an indication of the range of initial phase for the chaotic state.

One of the defining characteristics of the chaotic state is that, although the system will naturally relax to a chaotic trajectory, any particular chaotic trajectory is unstable with respect to small perturbations. More precisely, chaos is a steady-state behavior for which at least one Liapunov exponent is positive. Figure 11(b) plots the maximum Liapunov exponent λ for the solutions shown in Fig. 11(a). Over the range of $\tilde{i}_1$ where the solution is periodic, λ is negative, indicating stability in the presence of small perturbations. Above the accumulation point of the period-doubling cascade, λ is positive, confirming the chaotic nature of the solutions in this parameter range.

On the chaotic side of the accumulation point, one finds a reverse bifurcation cascade[49] in which the bands of chaotic motion shown in Fig. 11(a) gradually become wider and merge together, such that the number of bands will, at some point, decrease from 16 to 8, then from 8 to 4, and so on with increasing $\tilde{i}_1$. Usually, the envelopes of the chaotic bands widen smoothly but, as Fig. 11(a) shows, there are two discontinuities in the present instance. In the first discontinuity, at $\tilde{i}_1=2.3924$, the chaotic bands suddenly increase in width so that four bands merge to form two bands. In the second discontinuity, at $\tilde{i}_1=2.3934$, the chaotic bands suddenly disappear. Both of these discontinuities are produced by what are called crises[50] in which chaotic bands collide with unstable periodic solutions. The first crisis shown in Fig. 11 is called an interior crisis because the chaotic bands simply change size. The second is called an exterior crisis because it forms a boundary of the chaotic region.

Crises have been previously identified in the rf-biased junction by Sakai and Yamaguchi[31] and by Gwinn and Westervelt.[42] The nature of the collision between chaotic solutions and unstable periodic solutions is illustrated in Fig. 12. Here we show the Poincaré sections of the chaotic solution for values of $\tilde{i}_1$ just below the two crisis points. The Poincaré section is obtained by plotting the location of the system in state space at the beginning of a large number of successive rf cycles. At $\tilde{i}_1=2.392$ the Poincaré section [Fig. 12(a)] consists of four distinct segments, one for each of the four bands in Fig. 11(a). The circles shown in Fig. 12(a) locate the twelve points corresponding to an unstable period-12 solution. As $\tilde{i}_1$ increases beyond 2.392, the four segments of the chaotic solution expand until they collide with the unstable period-12 solution at $\tilde{i}_1=2.3924$ to produce the interior crises. Similarly, the exterior crisis at $\tilde{i}_1=2.3934$ results when the two segments of the chaotic solution shown in Fig. 12(b) collide with the indicated unstable period-6 solution.

Beyond the exterior crisis at $\tilde{i}_1=2.3934$, the system switches from a chaotic solution to a stable period-2 solution on the $n=1$ step. Thus, at $\Omega_1=0.14$, the chaotic region which evolves from the $n=0$ period-doubling cascade spans only the short interval from $\tilde{i}_1=2.3910$ to 2.3934. Moreover, the chaos which occurs on this interval is of a weak type which we describe as phase-locked

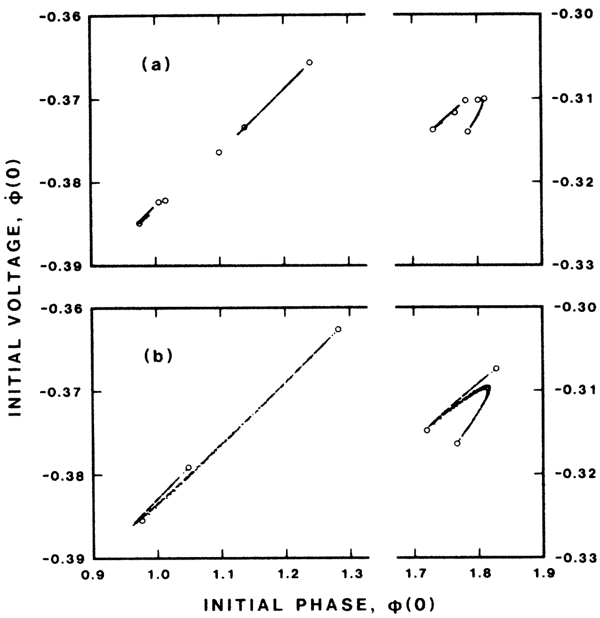

FIG. 12. Poincaré sections of chaotic attractors at (a) $\tilde{i}_1=2.392$ and (b) $\tilde{i}_1=2.393$ for $\beta=100$, $\Omega_1=0.14$, and $i_0=0$. Each Poincaré section plots the location of the system in state space at the beginning of 1024 successive rf cycles. Circles show the locations of two unstable periodic solutions, a period-12 solution in frame (a) and a period-6 solution in frame (b).

chaos[9,16,20,38] and is elsewhere described as chaos without diffusion[17] and narrow chaos.[31]. The chaotic solution is said to be phase locked because the phase maintains synchrony with the rf bias. In the present instance, the phase advances by 0 revolutions during each rf cycle, with small variations in $\phi(0)$ from cycle to cycle but no 2π phase slips. Phase-locked chaos is also characterized by a noise spectrum which approaches zero at low frequencies.[9,16,20,38] One concludes that the chaotic region shown in Fig. 11, which spans a narrow range of rf amplitudes and produces a relatively low level of noise, would be difficult to detect experimentally.

The chaotic region shown in Fig. 11 is typical of chaotic regions that evolve from a period-doubling cascade. When chaos evolves from a cascade associated with the nth rf-induced step, the chaotic solutions just beyond the accumulation point are phase locked and advance by n revolutions during each rf cycle. The phase-locked chaotic region usually spans a parameter range smaller than that of the cascade and is usually terminated by a crisis. All along the upper limit of branch A for $\Omega_1 \leq 1.4\Omega_p$ and the upper limit of branch B for $\Omega_1 \leq 1.69\Omega_p$ (cf. Fig. 3), one thus finds a narrow range of rf amplitudes where phase-locked chaos is observed. With the exception of the chaotic region adjoining branch A on the interval $0.66\Omega_p \leq \Omega_1 \leq 1.4\Omega_p$, the crisis which terminates this narrow interval of phase-locked chaos is invariably an exterior crisis, beyond which the system switches to a periodic solution. Thus, the chaotic regions adjoining branch A for $\Omega_1 \leq 0.66\Omega_p$ and adjoining branch B for $\Omega_1 \leq 1.69\Omega_p$, which include the chaotic regions for which the onset of chaos is accurately predicted by the method of Melnikov, are very limited in extent and would be difficult to observe experimentally.

In contrast, the chaotic region adjoining branch A on the interval $0.66\Omega_p \leq \Omega_1 \leq 1.40\Omega_p$ is at some points relatively easy to detect. In this frequency range, the crisis which ends the phase-locked chaotic region is often an interior crisis, beyond which unlocked chaos is observed. An example of this situation is shown in Fig. 13 for $\Omega_1=0.7\Omega_p$. The crisis occurs in this case at $\tilde{i}_1=1.1786$ where the phase-locked chaotic solution collides with an unstable period-5 solution. Beyond the crisis point, the solution remains chaotic but the phase no longer maintains synchrony with the rf bias, advancing by a variable number of revolutions per rf cycle. For unlocked chaos, also called chaos with diffusion[17] and wide chaos,[31] the initial phase can assume any value between $-\pi$ and π [cf. Fig. 13(a)] and the noise spectrum approaches a constant at low frequencies.[9,16,20,25,38] Thus, the noise produced by unlocked chaotic motion is much greater than that for phase-locked chaos, allowing easy experimental detection. Unlocked chaos is also easy to detect because it tends to span a much broader range of parameters than phase-locked chaos. In the present instance, phase-locked chaos is limited to the range of $\tilde{i}_1$ from 1.1772 to 1.1786 while unlocked chaos extends without significant interruption from $\tilde{i}_1=1.1786$ to 1.6284.

Because the chaos most easily detected in experiments is unlocked chaos, it is of interest to consider the rf-amplitude threshold for unlocked chaos. For frequencies

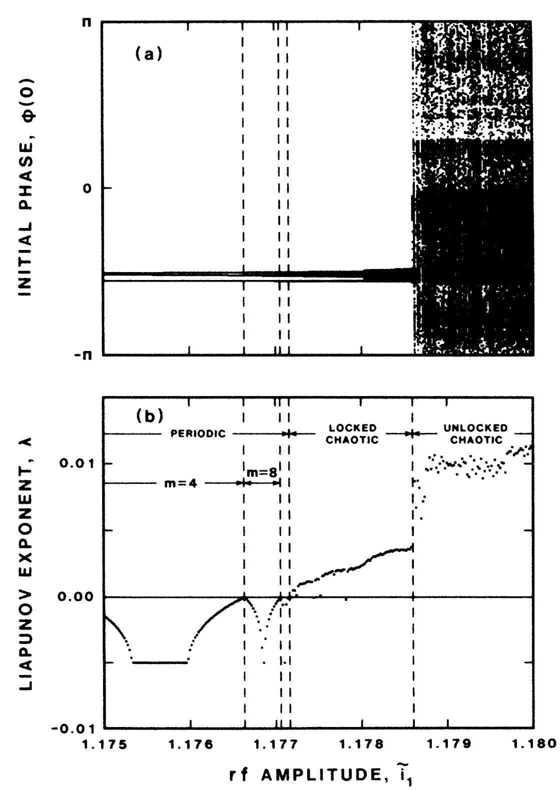

FIG. 13. Initial phase (a) and maximum Liapunov exponent (b) as a function of rf amplitude for $\beta=100$, $\Omega_1=0.07$, and $i_0=0$. For each rf amplitude, 512 values of $\phi(0)$ are plotted. λ is calculated over 8192 rf cycles.

between $0.66\Omega_p$ and $1.4\Omega_p$ the onset of unlocked chaos usually occurs at an rf amplitude near the upper bound of solution branch A. In some cases, as at $\Omega_1=0.7\Omega_p$, unlocked chaos begins immediately after the narrow interval of phase-locked chaos that adjoins branch A. In other cases, where the phase-locked chaotic region is bounded by an exterior crisis, unlocked chaos occurs only at somewhat higher values of $\tilde{i}_1$. At $\Omega_1=\Omega_p$, for example, branch A ends at $\tilde{i}_1=1.8076$, the associated region of phase-locked chaos ends at $\tilde{i}_1=1.8086$, periodic $n=1$ solutions are found between $\tilde{i}_1=1.8086$ and 2.1309 [cf. Fig. 6(b)], and the onset of unlocked chaos is at $\tilde{i}_1=2.1309$. Thus, while the rf-amplitude threshold for unlocked chaos is not a simple function of frequency, it is usually not far above the upper bound of branch A at frequencies between $0.66\Omega_p$ and $1.4\Omega_p$.

Similarly, at frequencies below $0.66\Omega_p$, the onset of unlocked chaos is usually close to the upper bound of solution branch C. As noted earlier, at $\Omega_1=0.5\Omega_p$ the onset of chaos does not occur at $\tilde{i}_1=2.99$, the upper limit of branch C. However, unlocked chaos does appear at $\tilde{i}_1=3.56$, a point not far above branch C. At $\Omega_1=0.6\Omega_p$, on the other hand, the onset of chaos coincides with the tangent bifurcation at $\tilde{i}_1=1.62644$ which ends branch C, as shown in Fig. 14. In this case, the scenario for the onset of chaos is the tangency or intermittency scenario which has often been observed in this system.[14,19,23–26,33,37] Thus, the situation for frequencies below $0.66\Omega_p$ is much like the situation for frequencies above $0.66\Omega_p$ except that the unlocked chaotic state is often entered through the tangency bifurcation which ends branch C rather than the period-doubling cascade which ends branch A.

Because the onset of unlocked chaos is close to the upper limit of branch C for $\Omega_1 \leq 0.66\Omega_p$ and close to the upper limit of branch A for $0.66\Omega_p \leq \Omega_1 \leq 1.4\Omega_p$ the experimentally observed onset of chaos is expected to roughly follow the "vee"-shaped curve in Fig. 3 which is defined by the upper limits of branches A and C. Such a "vee"-shaped threshold curve with a minimum in the neighborhood of $0.6\Omega_p$ has been obtained in many previous simulations[2,3,7,10,13,16,18,29] and is confirmed by experimental observations.[3,44] The previous studies show that the region above this "vee"-shaped curve includes broad areas of unlocked chaos interspersed with islands of periodic motion. In contrast, the chaotic region predicted by the method of Melnikov, which occurs at lower rf amplitudes, spans only a narrow parameter range and includes only weakly chaotic, phase-locked solutions. Although of theoretical interest, this latter region of chaos is unlikely to prove of practical significance.

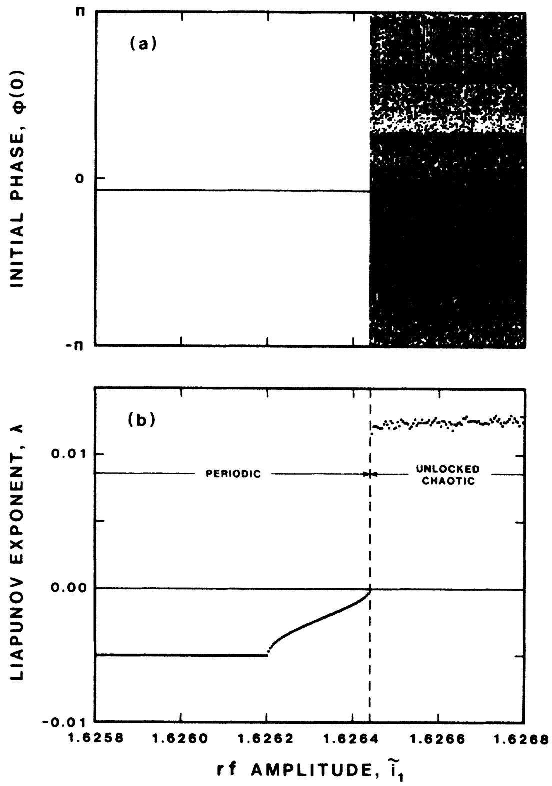

FIG. 14. Initial phase (a) and maximum Liapunov exponent (b) as a function of rf amplitude for $\beta=100$, $\Omega_1=0.06$, and $i_0=0$. For each rf amplitude, 512 values of $\phi(0)$ are plotted. λ is calculated over 8192 rf cycles.

ACKNOWLEDGMENT

This work was carried out while R. L. Kautz was at the CSIRO Division of Applied Physics in Sydney, Australia; he would like to thank the CSIRO staff for their hospitality during his stay.

[1]V. N. Belykh, N. F. Pedersen, and O. H. Soerensen, Phys. Rev. B **16**, 4860 (1977).
[2]Z. D. Genchev, Z. G. Ivanov, and B. N. Todorov, IEEE Trans. Circuits Syst. **CAS-30**, 633 (1983).
[3]V. N. Gubankov, S. L. Ziglin, K. I. Konstantinyan, V. P. Koshelets, and G. A. Ovsyannikov, Zh. Eksp. Teor. Fiz. **86**, 343 (1984) [Sov. Phys.—JETP **59**, 198 (1984)].
[4]F. M. A. Salam and S. S. Sastry, in *IEEE 1984 International Symposium on Circuits and Systems Proceedings* (IEEE, New York, 1984), p. 860; IEEE Trans. Circuits Syst. **CAS-32**, 784 (1985).
[5]M. Odyniec and L. O. Chua, IEEE Trans. Circuits Syst. **CAS-32**, 34 (1985).
[6]Y. Braiman, E. Ben-Jacob, and Y. Imry, in *SQUID '80*, edited by H. D. Hahlbohm and H. Lubbig (de Gruyter, Berlin, 1980), p. 783.
[7]B. A. Huberman, J. P. Crutchfield, and N. H. Packard, Appl. Phys. Lett. **37**, 750 (1980).
[8]E. Ben-Jacob, Y. Braiman, R. Shainsky, and Y. Imry, Appl. Phys. Lett. **38**, 822 (1981).
[9]R. L. Kautz, J. Appl. Phys. **52**, 6241 (1981).
[10]N. F. Pedersen and A. Davidson, Appl. Phys. Lett. **39**, 830 (1981).
[11]M. T. Levinsen, J. Appl. Phys. **53**, 4294 (1982).
[12]W.-H. Steeb and A. Kunick, Phys. Rev. A **25**, 2889 (1982).
[13]M. Cirillo and N. F. Pedersen, Phys. Lett. **90A**, 150 (1982).
[14]E. Ben-Jacob, I. Goldhirsch, Y. Imry, and S. Fishman, Phys. Rev. Lett. **49**, 1599 (1982).
[15]W. J. Yeh and Y. H. Kao, Phys. Rev. Lett. **49**, 1888 (1982).
[16]D. D'Humieres, M. R. Beasley, B. A. Huberman, and A. Lib-

chaber, Phys. Rev. A **26**, 3483 (1982).
[17]M. Inoue and H. Koga, Prog. Theor. Phys. **68**, 2184 (1982).
[18]A. H. MacDonald and M. Plischke, Phys. Rev. B **27**, 201 (1983).
[19]W. J. Yeh and Y. K. Kao, Appl. Phys. Lett. **42**, 299 (1983).
[20]R. L. Kautz, IEEE Trans. Magn. **MAG-19**, 465 (1983).
[21]Y. Imry, in *Statics and Dynamics of Nonlinear Systems,* edited by G. Benedek, H. Bilz, and R. Zeyher (Springer, Berlin, 1983), p. 170.
[22]Z. J. Kowalik, Acta Phys. Pol. A **64**, 357 (1983).
[23]H. Koga, H. Fujisaka, and M. Inoue, Phys. Rev. A **28**, 2370 (1983).
[24]H. Seifert, Phys. Lett. **98A**, 213 (1983).
[25]M. Octavio, Phys. Rev. B **29**, 1231 (1984).
[26]I. Goldhirsch, Y. Imry, G. Wasserman, and E. Ben-Jacob, Phys. Rev. B **29**, 1218 (1984).
[27]H. Seifert, Phys. Lett. **101A**, 230 (1984).
[28]D.-R. He, W. J. Yeh, and Y. H. Kao, Phys. Rev. B **30**, 172 (1984).
[29]A. Aiello, A. Barone, and G. A. Ovsyannikov, Phys. Rev. B **30**, 456 (1984).
[30]P. Bak, T. Bohr, H. Jensen, and P. V. Christiansen, Solid State Commun. **51**, 231 (1984).
[31]K. Sakai and Y. Yamaguchi, Phys. Rev. B **30**, 1219 (1984).
[32]M. Octavio and C. R. Nasser, Phys. Rev. B **30**, 1586 (1984).
[33]H. Seifert and C. Noldeke, in *Proceedings of the 17th International Conference on Low Temperature Physics LT-17,* edited by U. Eckern, A. Schmid, W. Weber, and H. Wuhl (North-Holland, Amsterdam, 1984), p. 1135.
[34]E. G. Gwinn and R. M. Westervelt, in *Proceedings of The 17th International Conference on Low Temperature Physics LT-17,* edited by U. Eckern, A. Schmid, W. Weber, and H. Wuhl (North-Holland, Amsterdam, 1984), p. 1139.
[35]T. Bohr, P. Bak, and M. H. Jensen, Phys. Rev. A **30**, 1970 (1984).
[36]M. J. Kajanto and M. M. Salomaa, Solid State Commun. **53**, 99 (1985).
[37]D.-R. He, W. J. Yeh, and Y. H. Kao, Phys. Rev. B **31**, 1359 (1985).
[38]R. L. Kautz and R. Monaco, J. Appl. Phys. **57**, 875 (1985).
[39]T. Geisel, J. Nierwetberg, and A. Zacherl, Phys. Rev. Lett. **54**, 616 (1985).
[40]D. C. Cronemeyer, C. C. Chi, A. Davidson, and N. F. Pedersen, Phys. Rev. B **31**, 2667 (1985).
[41]Q. Hu, J. U. Free, M. Iansiti, O. Liengme, and M. Tinkham, IEEE Trans. Magn. **MAG-21**, 590 (1985).
[42]E. G. Gwinn and R. M. Westervelt, Phys. Rev. Lett. **54** 1613 (1985).
[43]R. L. Kautz, J. Appl. Phys. **58**, 424 (1985).
[44]V. N. Gubankov, K. I. Konstantinyan, V. P. Koshelets, and G. A. Ovsyannikov, Pis'ma Zh. Tekh. Fiz. 8, 1332 (1982) [Sov. Tech. Phys. Lett. **8**, 574 (1982)]; IEEE Trans. Magn. **MAG-19**, 637 (1983).
[45]C. R. Nasser and M. Octavio, in *Proceedings of the 17th International Conference on Low Temperature Physics LT-17,* edited by U. Eckern, A. Schmid, W. Weber, and H. Wuhl (North-Holland, Amsterdam, 1984), p. 1129.
[46]W. C. Stewart, Appl. Phys. Lett. **12**, 277 (1968).
[47]D. E. McCumber, J. Appl. Phys. **39**, 3113 (1968).
[48]S. Rudner, M. J. Feldman, E. Kollberg, and T. Claeson, J. Appl. Phys. **52**, 6366 (1981).
[49]A. J. Lichtenberg and M. A. Lieberman, *Regular and Stochastic Motion* (Springer, New York, 1983).
[50]C. Grebogi, E. Ott, and J. A. Yorke, Physica **7D**, 181 (1983).
[51]R. L. Kautz, J. Appl. Phys. **52**, 3528 (1981).
[52]*Handbook of Mathematical Functions,* edited by M. Abramowitz and I. A. Stegun (Dover, New York, 1965), p. 589.

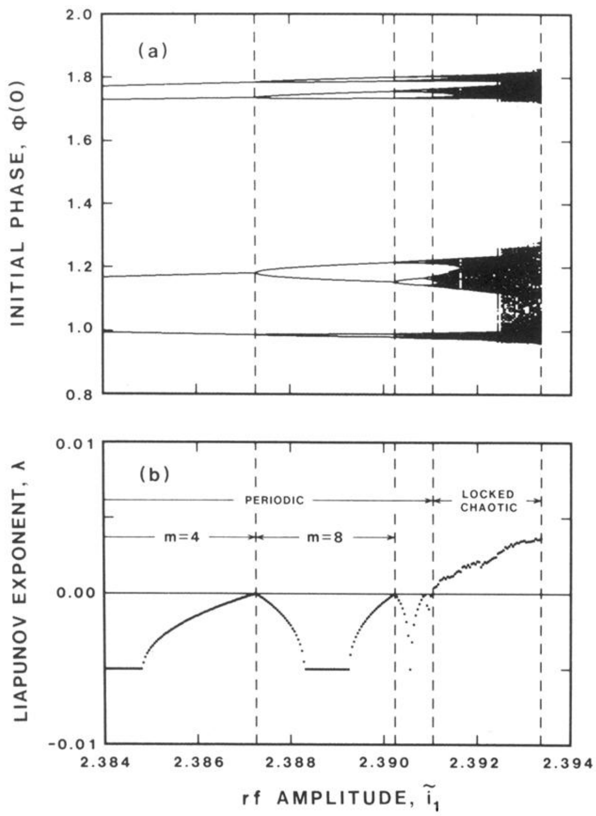

FIG. 11. Initial phase (a) and maximum Liapunov exponent (b) of the steady-state solution as a function of rf amplitude for $\beta = 100$, $\Omega_1 = 0.14$, and $i_0 = 0$. For each rf amplitude, the phase at the beginning of 512 successive rf cycles is plotted in frame (a). The maximum Liapunov exponent is calculated over 8192 rf cycles.

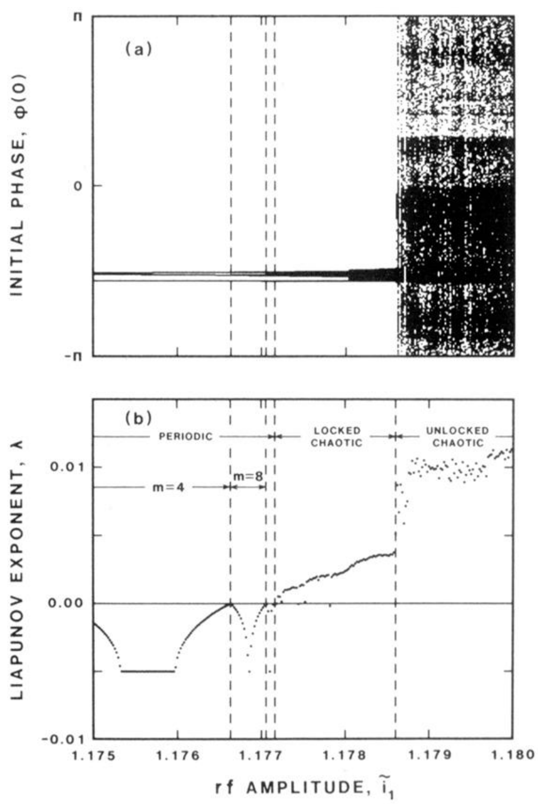

FIG. 13. Initial phase (a) and maximum Liapunov exponent (b) as a function of rf amplitude for $\beta=100$, $\Omega_1=0.07$, and $i_0=0$. For each rf amplitude, 512 values of $\phi(0)$ are plotted. λ is calculated over 8192 rf cycles.

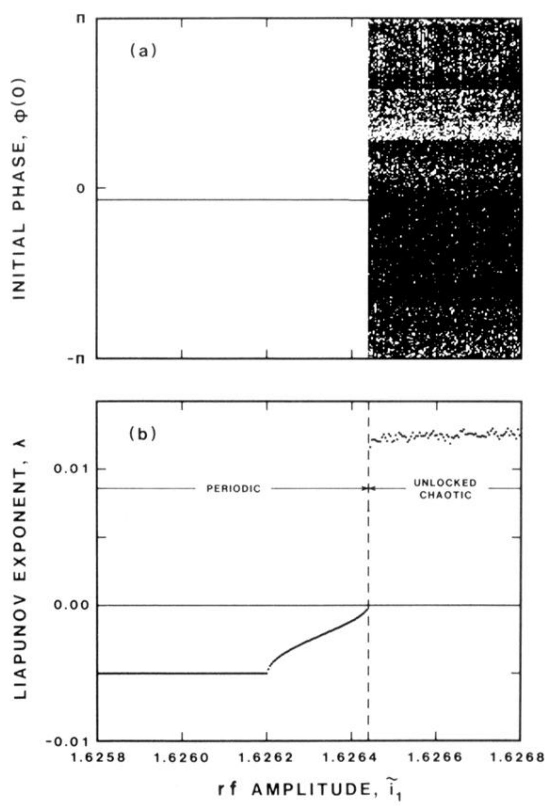

FIG. 14. Initial phase (a) and maximum Liapunov exponent (b) as a function of rf amplitude for $\beta=100$, $\Omega_1=0.06$, and $i_0=0$. For each rf amplitude, 512 values of $\phi(0)$ are plotted. λ is calculated over 8192 rf cycles.